Study of gamma backscattering in a multielemental medium

Martha Liliana Cortés, Fernando Cristancho

Departamento de Física, Universidad Nacional de Colombia, Bogotá, Colombia
Centro Internacional de Física CIF, Bogotá, Colombia
(Dated: December 17 of 2007)

The idea of constructing an instrument based in γ–ray backscattering that allows obtaining images similar to the produced with X rays, was recently proposed. The materialization of such idea needs a study of the flux of backscattered photons in a multielemental medium and of the different processes that contribute to the total result. By means of analytical approximations we find estimates of the contribution of the most important processes involved in the γ–soil interaction. We find an optimal energy around 250 keV for which the number of backscattered photons is higher. We characterize tansmission and backscattering spectra and finally we compare our experimetnal results with `Geant4` simulations.

I. INTRODUCTION

Big efforts have been undertaken recently in detection of organic materials buried in the soil. Several methods have been proposed to this aim, for example nuclear reactions and neutron backscattering. One of these methods based on γ–ray backscattering was recently proposed[1]. That method is based on the linear dependence of the number of backscattered photons with the electron density of the medium. The development of this method is been carried out by the GSI of Darmstadt, Germany in collaboration with the grupo de física nuclear de la Universidad Nacional de Colombia (gfnun). The proposed scheme[1] is shown in Figure 1. A ^{22}Na source is placed in a conical lead shielding. In the top of the shielding is placed a position–sensitive detector. A ring–shaped detector is enclosing the source and is used as a backscattering detector. The ^{22}Na emits positrons which rapidly annihilate with an electron. The result of this process is the emission of two photons of 511 keV moving in opposite directions. One of these photons

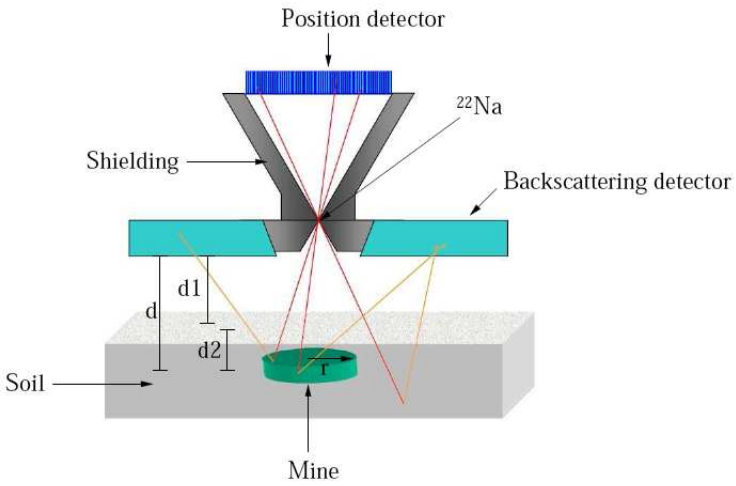

FIG. 1. Scheme for the detection of organic material using positron annihilation

can be detected in the position detector, the other one goes into the soil where it can be absorbed or scattered. If the photon is backscattered it can be detected in the backscattering detector. The number of backscattered photons depends on the electron density of the soil, therefore we should be able to detect electron density differences in the soil. It is important to take into account that besides the positron, the ^{22}Na source emits a γray of 1275 keV which can interfere with the measurements. Figure 2 shows the decay scheme of ^{22}Na.

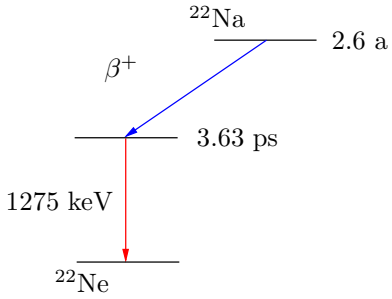

FIG. 2. Decay scheme for ^{22}Na

In order to improve the instrument performance it is essential to study carefully the γ–soil interaction. In the present report we center our attention in the characteristics of the soil and in its response to γ–rays. For this purpose we use a simplified model to describe this interaction by means of three different approaches: Analytical, experimental and a comparison with simulations. We find estimates of the relevance of each physical process involved in the interaction and its contribution to the number of backscattered photons as a function of the depth. We also find the optimum energy range for which the backscattering probability reaches a maximum. With the corresponding experimental set–up we obtain and characterize transmission and backscattering spectra for different widths of soil layers. Finally we compare our experimental results with `Geant4` simulations.

II. THEORETICAL ASPECTS

The theoretical study of γ–backscattering in the soil is mainly based on two phenomena: The total attenuation coefficient of the beam in the soil and the angular scattering probability.

A. Total attenuation coefficient

The linear attenuation coefficient gives us the probability for γ–rays to interact with any material per unit length as a function of energy. This attenuation coefficient can be expresses as

$$\mu = n\left(\sigma_{ph} + Z\sigma_C + \sigma_{pp}\right), \tag{2.1}$$

where n is the number of scattering centers per unit volume, σ_{ph} is the photoelectric effect cross section, Z is the number of electrons per scattering center, σ_C is the Compton effect cross section and σ_{pp} is the pair production cross section. This coefficient determines the intensity I of a γ–ray beam after passing through a distance x of any material according to

$$I(x) = I_0 e^{-\mu x}, \tag{2.2}$$

where I_0 is the incident beam intensity. If we divide the linear attenuation coefficient by the mass density of the medium we are considering, we obtain the mass attenuation coefficient. The units of the mass attenuation coefficient then are cm^2/g. Clearly the value of this coefficient depends not only on the energy of the beam, but also on the medium we considere.

Figure 3 shows the mass attenuation coefficient for the interaction γ–soil for a soil composed of SiO_2. This composition corresponds to a soil of dry sand. We choose this composition because the experiments were carried out with dry sand. We can see from this figure that as the energy increases the mass attenuation coefficient decreases. This would imply that if we increase the energy of the incident photons we would obtain smaller attenuation, and therefore more penetration of the γrays in the soil. However, we will see later that the increase of the penetration does not implies an increase of the total number of backscattered photons. This figure also shows the interaction probability for each of the possible process for which the photons can interact: Photoelectric effect, Compton effect and pair production. We can see that for both 0.511 MeV and 1.275 MeV the highest interaction probability is the one corresponding to Compton effect.

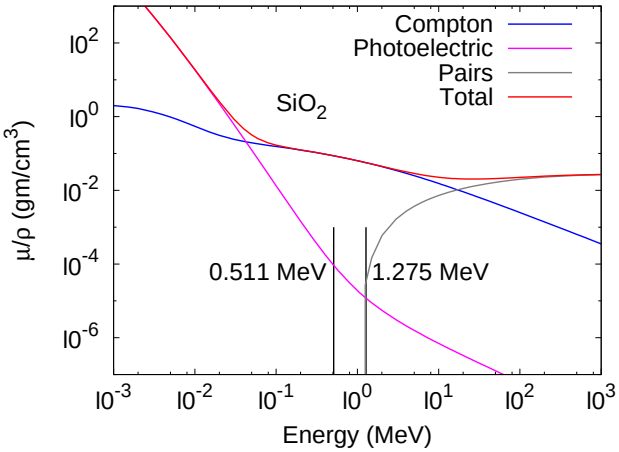

FIG. 3. Total attenuation coefficient for interaction γ–soil for a soil composed of SiO_2

B. The Klein–Nishina formula

The scattering probability of a photon of incident energy E_γ in a solid angle $d\Omega$ around an angle θ as a function of the scattering angle is given by the Klein–Nishina formula (2.3)

$$\frac{d\sigma}{d\Omega} = \frac{r_e^2}{2}\frac{1}{[1+\gamma(1-\cos\theta)]^2}\left(1+\cos^2\theta+\frac{\gamma^2(1-\cos\theta)^2}{1+\gamma(1-\cos\theta)}\right), \tag{2.3}$$

where r_e is the classical radius of the electron, $\gamma = E_\gamma/511$ keV and θ is the angle between the direction of the incident photon and the photon scattering direction. Figure 4 shows a polar plot of the Klein–Nishina formula for different incident energies. We can see from the figure that the scattering probability is higher for angles between $-\pi/2$ and

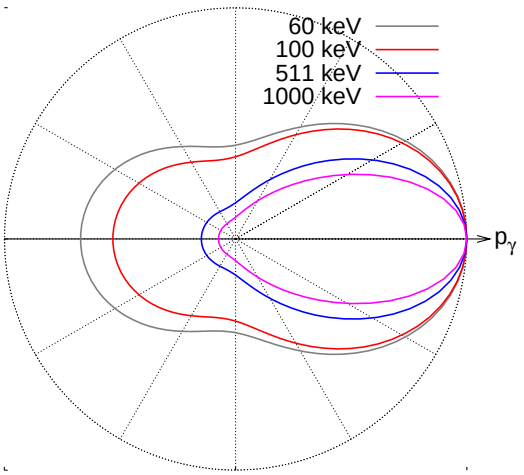

FIG. 4. Polar plot of the Klein–Nishina formula for different energies. $\theta = 0$ corresponds to the incident direction of the photon

$\pi/2$. We can also see that when increase the energy the backscattering probability, i.e. the probability for a photon to scatter within $\pi/2 \leq \theta \leq 3\pi/2$, decreases. Therefore by reducing the incident energy of the radioactive source we

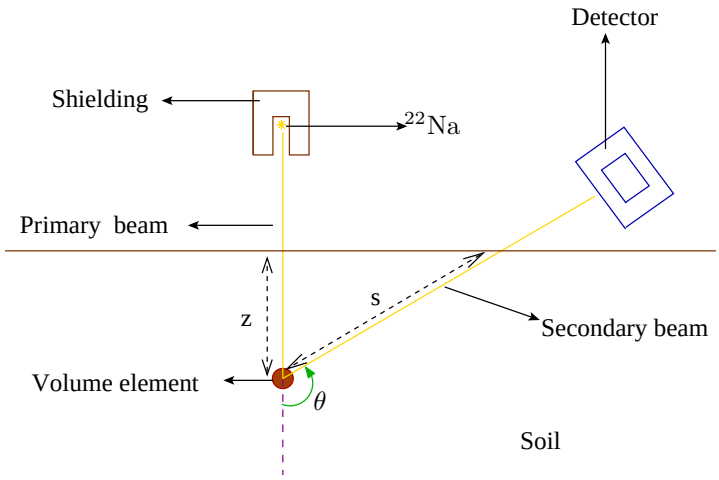

FIG. 5. Simplified model for studying the γ–soil interaction

obtain a higher backscattering probability. Nevertheless according to section II A if we diminished the incident energy we would have a larger mass attenuation coefficient. This is the reason why the number of backscattered photons will not increase. As a conclusion, the total number of backscattered photons is mainly the result of the combination of two effects: The attenuation of the beam and the backscattering probability.

III. ANALYTICAL APPROACH

As a first approximation to obtain the number of backscattered photons in the soil we use an analytical approach: The huge equation method. Let us consider a soil of uniform composition of SiO_2 and constant density $\rho = 1.5$ g/cm^3. The simplified experimetnal set–up we use is shown in Figure 5. The idea of the method is to find estimates of the number of photons backscattered in each volume element as a function of depth z. We divide the soil in volume elements of area $A = 1$ cm^2 and depth $dz = 0.1$ cm. According to this method, the number of backscattered photons in a volume element dV at a depth z per unit time is

$$\delta S = \mathrm{N}_0 e^{-\mu z} \sigma_C \frac{d\sigma}{d\Omega} \Delta\Omega \rho_e dV e^{-\mu' s} + M, \tag{3.1}$$

where N_0 is the number of incident photons per unit area per unit time, μ is the linear attenuation coefficient of the soil for the incident energy, $\Delta\Omega$ is the solid angle subtended by the detector from the volume element, ρ_e is the electron density in the volumen element, $dV = Adx$ is the volume element, μ' is the linear attenuation coefficient for the scattered photon and s is the distance between the volume element and the soil surface, therefore the number $\frac{d\sigma}{d\Omega}\Delta\Omega\rho_e dV$ represents the angular scattering probability. M is the contribution of multiple scattering. In the calculation we use an ideal detector of 3.8 cm of radius placed 4 cm to the right of the source and 0.1 cm above the soil. In this case we neglect the multiple scattering contribution. Figure 6 shows the results of the calculation for three different beam energies. Figure 6(a) shows the number of backscattered photons as a function of depth taking into account the angular scattering probability which depends only on the geometrical configuration. Figure 6(b) shows the number of backscattered photons as a function of depth taking also into account the effect of the beam attenuation in both primary and secondary beams. We can see that the inclusion of the attenuations causes the number of counts to decrease in about two orders of magnitude. This inclusion also causes a shift of the depth which has a higher backscatter. This means that attenuation shifts the depth for which we obtain better information. The value of this shift depends on the linear attenuation coefficient which also depends on the beam energy as shown in Figure 3 and we can see that the lower the energy the higher the shift.

Additionally from Figure 6(a) we can see that for lower energies the number of backscattered photons is higher, but when we include the attenuations effect this behavior changes: although the number of counts is larger for 511 keV than for 1275 keV, as in the non–attenuation case, the number of counts for 60 keV is smaller than for 511 keV.

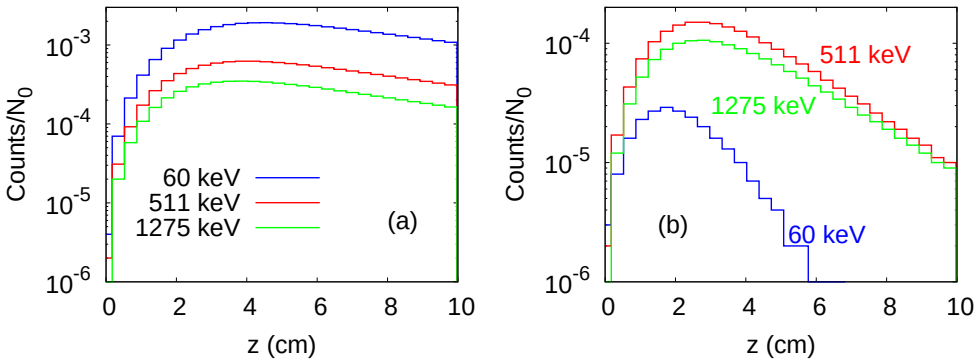

FIG. 6. Number of backscattered photons in function of the depth for three different beam energies. (a) Effect of the angular scattering probability. (b) Result taking into account the effect of attenuation of the beam

This fact suggest the existence of an optimum energy for which the number of backscattered photons is maximum. Figure 7 shows the total number of counts as a function of the incident energy, this number is obtained by integration of the counts over all depths. We can see that there is a range around 250 keV for which the number of counts is

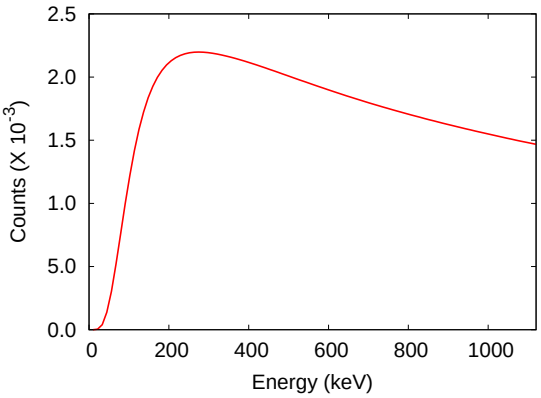

FIG. 7. Number of backscattered photons as a function of incident energy

larger. This means that it would be ideal to use γ–rays with energies near 250 keV, however as our method is based in positronic annihilation we are limited to an energy of 511 keV.

Although we have obtained estimates of the relevance of the attenuation effect in the backscattering process, this calculations are still an approximation. One of the most important effects that we have neglected is the multiple scattering, but the inclusion of such effect in theoretical calculations can result very complicated. To start studying the multiple scattering probability and to characterize in a more realistic way the backscattering process we need to perform experiments.

IV. EXPERIMENTAL RESULTS

A. Electronics optimization

The first step to obtain and characterize the transmission and backscattering spectra, is to optimize the electronic configuration of the system to get the largest possible number of counts per second. For this purpose we use the experimental set–up shown in Figure 8. A ^{22}Na source of 18.5 kBq of activity is placed between a Sodium Iodine

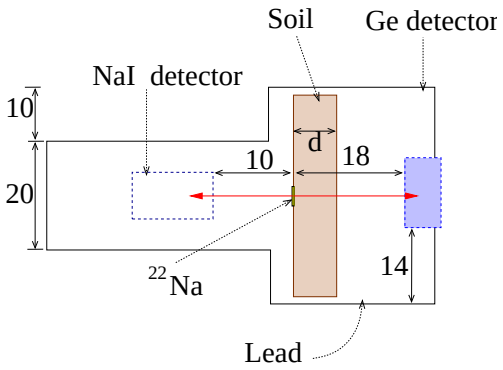

FIG. 8. Experimental setup used for the electronic optimization. All the lenghts are in cm

(NaI) and a Germanium (Ge) detector. Both detectors and the source are on a floor of lead.

As it was previously said, the ^{22}Na source emits positrons that annihilate and produce two gamma rays of 511 keV in opposite directions. If one of these γ–rays is detected in the NaI detector we have the possibility of detecting the other ray simultaneously in the Ge detector. The number of simultaneous events (coincidences) gives us information about the transmission of 511 keV gamma rays through any layer of soil that we place between the source and the Ge detector. In this case, as we are only interested in the optimization of the electronics, this medium was just air. This number of coincidences depends on the specific configuration of the electronics, i.e., on the different processes that the signals, originated in the detectors, go through.

1. Description of the electronics

Figure 9 shows a block diagram of the electronics configuration.

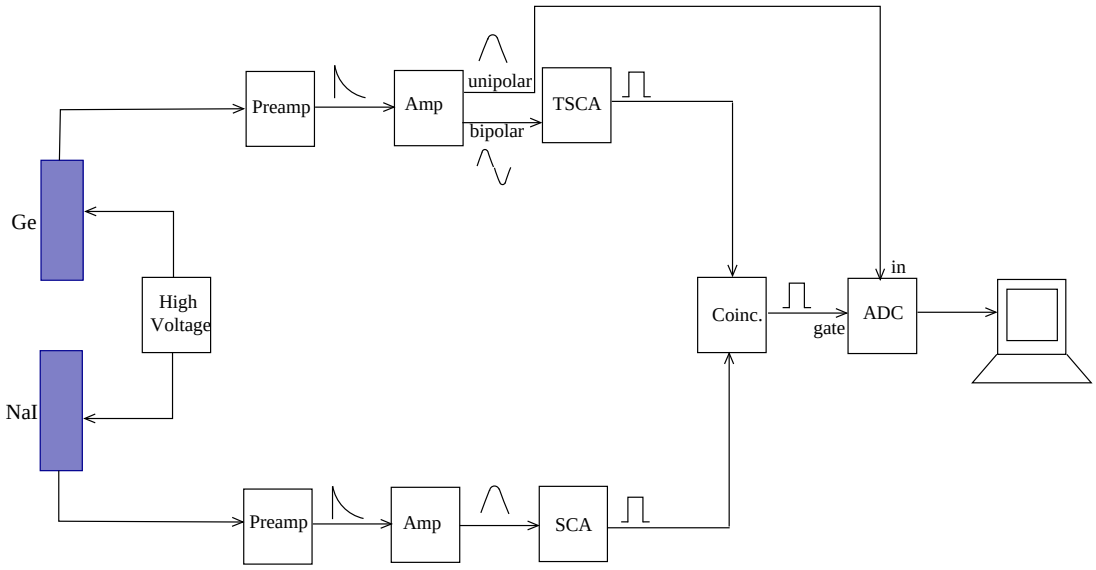

FIG. 9. Block diagram for the system electronics

The charge signal originated in each detector is converted in a tail voltage signal in a preamplifier. The height of this signal is proportional to the energy deposited in the detector. The next step is to convert this tail signal to a gaussian

shape and amplify it, which is done in the amplifier. The height of the gaussian is also proportional to the deposited energy and the output of the amplifier can be unipolar (composed by only one lobe) or bipolar (composed by two lobes). In the case of the Ge detector we use the unipolar output as the input of an Analog to Digital Converter (ADC) and connect the bipolar output to a Timing Single Channel Analyzer (TSCA), which emits a square pulse whenever the peak of the input gaussian fits in a certain range of values. It also has the possibility of delaying the output signal. For the NaI detector we only use the unipolar output as the input of a Single Channel Analyzer (SCA) which works in the same way as the TSCA (But without the delay possibility). Once we have the square pulses we connect them to the Coincidences module. This module emits a square pulse when the time difference between inputs is less than a parameter known as Resolving Time. This square pulse is connected to the gate input of the ADC, causing that the ADC only process gaussian inputs that arrive simultaneously with a coincidences pulse. This gaussian signals are sent to a Multichannel Analyzer (MCA) and finally to the computer where we can see the spectrum of coincidences.

By changing the parameters of the electronics we can find the configuration in which we obtain the major number of coincidences per minute.

2. Number of coincidences as a function of Resolving Time and TSCA's delay

The first parameter we vary is the delay of the TSCA module, that is the delay time between the moment at which the bipolar signal from the amplifier crosses the zero voltage line and the moment at which the square pulse is emitted. We performed this measurement for three different values of the Resolving Time in the coincidences module.

We can distinguish two different types of coincidences: Those that forms the 511 keV peak, and those that form the rest of the spectrum. Figure 10 shows the number of coincidences in the 511 keV peak as a function of TSCA's delay for different values of the Resolving Time.

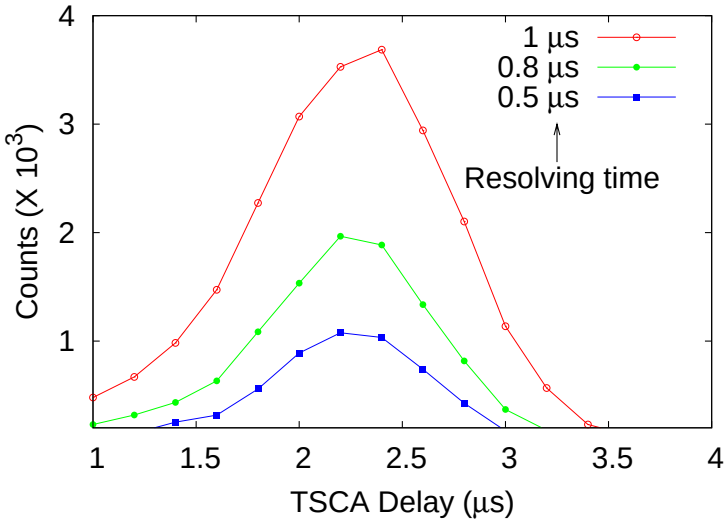

FIG. 10. Number of coincidences as a function of TSCA's delay for three different values of Resolving Time. The total measurement time was 5 minutes.

Clearly the largest number of counts is obtained for a Resolving Time of 1 μs, indicating that this is the value that maximize the number of counts. The peak of the curve is around 2.3 μs.

3. Number of coincidences as a function of ADC's delay

Once we have the optimal value for the Resolving Time we want to know the optimal value for the ADC's delay. This delay time corresponds to the maximum time difference between the gaussian input and the pulse in the gate input that the ADC stills considers a coincidence. With the TSCA's delay fixed to 2.3 μs (the value corresponding

to the maximum in figure 10), Resolving Time on 1 μs and leaving the rest of the electronic parameters unchanged we varied the ADC's delay and register the number of counts in the 511 keV peak. Figure 11 shows this number of coincidences as a function of ADC's delay.

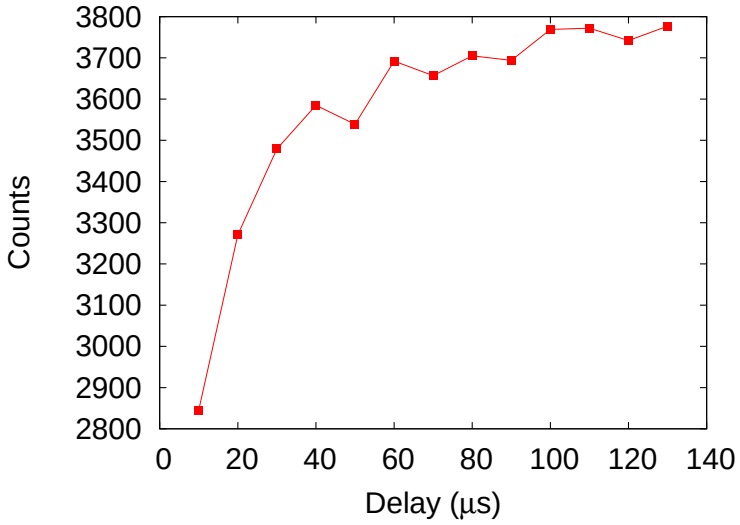

FIG. 11. Number of coincidences as a function of ADC's delay. The total measurement time was 5 minutes.

We see from the figure that the number of coincidences increases with the delay and tends to a maximum. We decide to use as optimal ADC's delay 100 μs.

B. Transmission experiments

For transmission experiments we use the same set–up shown in Figure 8 and measure the number of coincidences for 5 hours varying the thickness d of sand between the source and the Ge detector. If there were no sand between the source and the Ge detector the energy spectrum obtained in the Ge would be like the one shown in figure 12. We would have gaussian peaks at 511 keV and 1275 keV, corresponding to the photons, coming from the positron annihilation and from the decay of ^{22}Ne, that leave all their energy in the detector, and a Compton region corresponding to the recoil electrons of γrays that suffer Compton effect into the detector. As it is expressed in equation (2.2) by measuring the transmitted intensity of the beam for different values of d we can find the value of the attenuation coefficient. To achieve this we calculate the number of 511 keV γ–rays in each spectrum and fit an exponential dependence with the sand thickness. Figure 13 shows the semi–log plot of the number of transmitted 511 keV photons as a function of soil thickness and the exponential fit. The fit gives us a value $\mu = 0.131(3)$ cm^{-1}. This value differs only 1.5% of the reported for SiO_2[2] thus we can, in good approximation, assume that our soil was mainly composed of this compound.

The main effect of putting layers of sand between the source and the Ge detector is that the photons emitted by the source can interact with the sand in the container before arriving to the detector, thus leaving an energy smaller than its incident energy. This effect can be observed along all the spectrum. The variation on the spectra due to the different sand thickness can be easily observed if we normalize the spectrum to the photopeak amplitude, i.e., if we divide the number of counts of each energy by the photopeak amplitude. Figure 14 shows a comparison of the normalized transmission spectra for air and two different layers of soil. Figure 14(a) shows the result of the normalization. We can see an increment in the relative number of counts along all the spectrum. If we look closer, as in Figure 14(b), we can see that as the sand thickness gets larger a higher broad peak is observed in the Compton region. The energy of this peak is around 100 keV. The appearing of this peak is due to the cumulative effect of multiple dispersion in the sand, backscattering of photons in the detector and backscattering of already scattered photons.

We can also see a formation of a tail in the low energy side of the 511 keV photopeak. This tail increases with the sand thickness and is mainly due to the detection of small–angle scattered photons. A second way to observe the

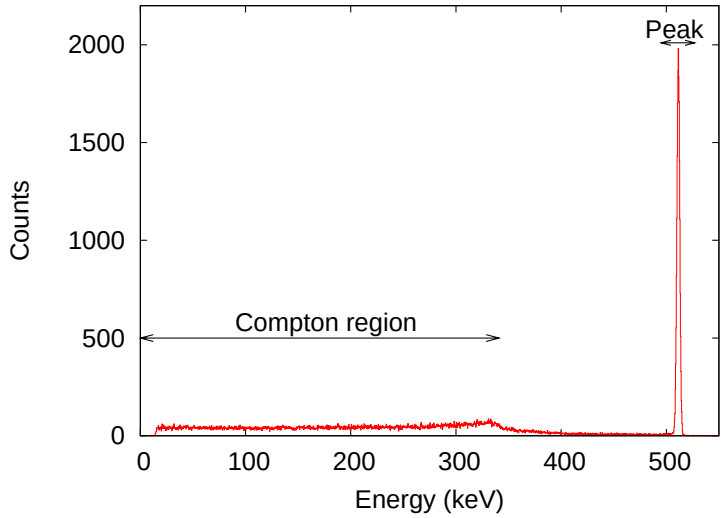

FIG. 12. Energy spectrum of ^{22}Na in the Ge detector

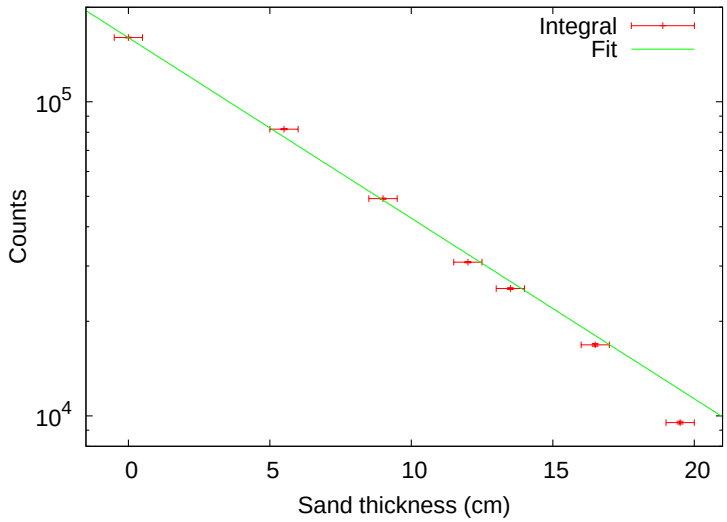

FIG. 13. Number of transmitted γrays of 511 keV as a function of sand thickness. Each measurement was of 5 hours

effect of sand in the spectrum is to divide it in regions as shown in Figure 15: the Compton region from 0 keV to the 511 keV Compton (341 keV), the interval region from 342 keV to 500 keV and the photopeak region from 501 keV to 522 keV. If we plot the number of counts in each region as a function of the sand thickness we obtain the results shown on Figure 16. In this Figure we can see that the number of counts in the photopeak has an exponential dependence which is in good agreement with the exponential attenuation shown in equation (2.2) with a slope corresponding to the linear attenuation coefficient found previously. This exponential behavior is not seen for the Compton and interval regions which besides of having a lower slope than the observed for the photopeak, we can see a change in the slope around 12 cm. The fact that the slopes for the Compton and interval regions do not correspond to the calculated linear attenuation coefficient indicates that the number of counts in these regions is affected by other phenomena apart from attenuation. We still do not have a clear explanation for the observed change in the slopes of these regions around 12 cm.

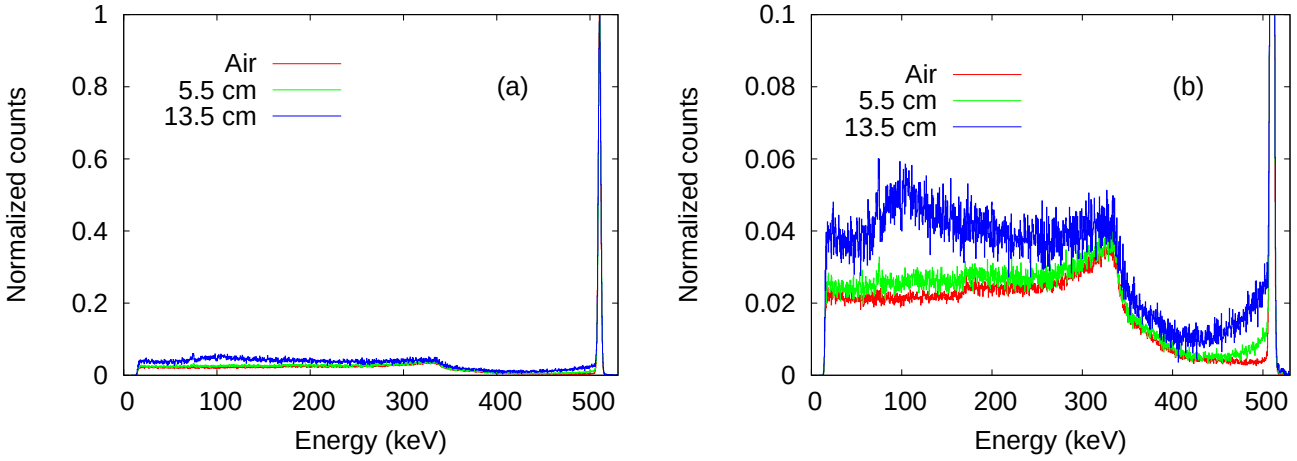

FIG. 14. Transmission espectra for differnt sand thickness. (a) Complete spectrum obtained (b) Zoom to the spectrum where we can see the effect of sand layer

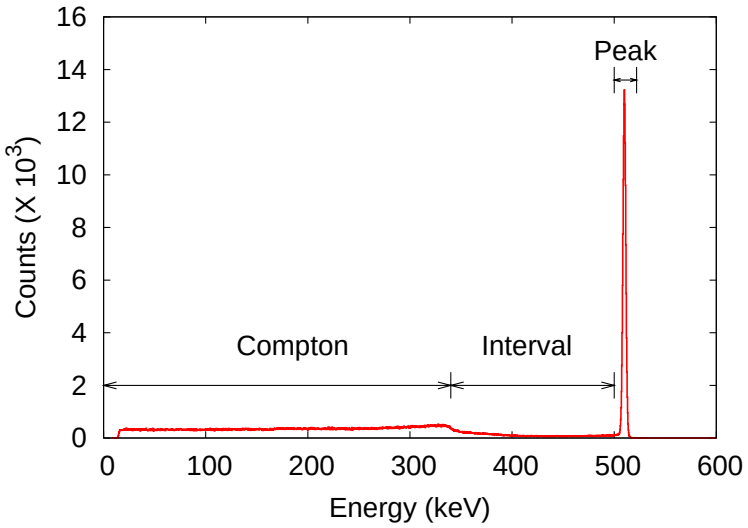

FIG. 15. Regions of the transmission spectrum

C. Backscattering experiments

In order to carry out backscattering experiments we use the experimental set–up shown in Figure 17: The angle between the incidence direction of the beam and the Ge detector is of $\theta = 148°$ and 5 cm of lead are placed between the source and this detector. In this case we count the number of backscattered photons in the direction of the detector. When carrying out the experiments for different sand thickness we observed that for $d > 5$ cm the obtained spectra show no difference, hence our analysis will be focused to thicknesses smaller than this critical value.

To analyze the backscattering spectra we divide them into three regions as shown in Figure 18: the Compton region from 0 keV to 180 keV, the peak region from 181 keV to 210 keV and the interval region from 211 keV to 500 keV. The Compton region corresponds to photons that may or may not interact with the sand and are backscattered towards

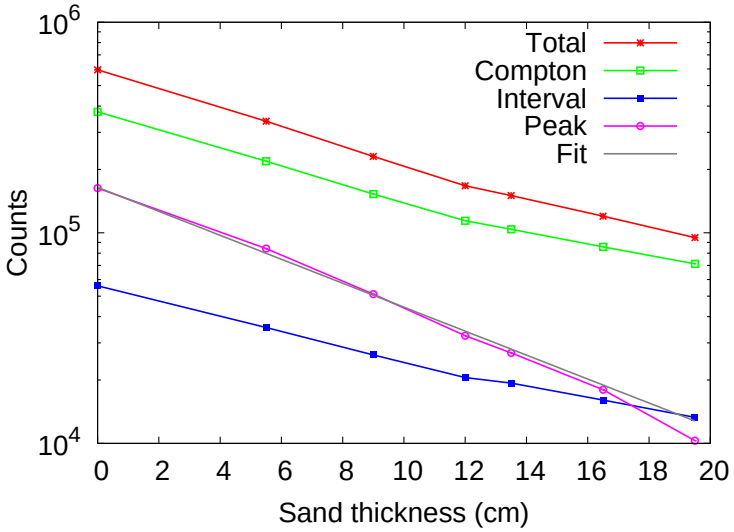

FIG. 16. Number of counts as a function of sand thickness

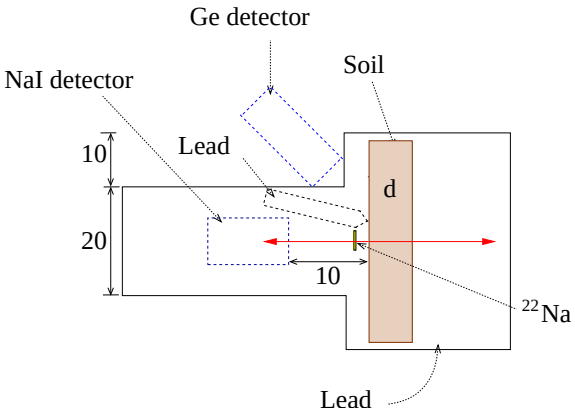

FIG. 17. Backscattering experimental setup

the detector where they interact via Compton effect leaving only part of its energy in the Ge detector. In this region we can also see a couple of lines at energies near 75 keV. These lines belong to the K_α emission of lead and they appear because of the photoelectric effect of the γrays.

The peak region is formed for the photons which are backscattered in the sand and are completely absorbed by the detector. If a photon would interact only once in the sand and then would be completely absorbed in the detector we would find a corresponding energy of 179 keV, however we observed a peak for an energy of 197 keV. This shift in the peak's energy is mainly due to three effects: photons carrying out multiple scattering in sand and later being detected, the finite size of the detector which allows the detection of photons scattered in a wide range of angles and not only in one angle and the coincidence between a 511 keV photon in the NaI detector and a 1275 photon backscattered in the sand.

The interval region is mainly composed of backscattering of 1275 keV photons. Additionally the spectrum has counts in the 511 keV photopeak. This is expected because, although there is a thick layer of lead between the source and the Ge detector, 511 keV photons have a finite probability of passing through the lead and be detected.

If we follow the same procedure as in the transmission case we can obtain the number of counts in each region of the spectrum for different values of sand thickness, however up to the moment of writing this report, we have data for only three thickness values. The result is shown in Figure 19. We can see a small increment in the number of counts for the Compton and the peak regions. This increment is due to the enhancement of the backscattering probability

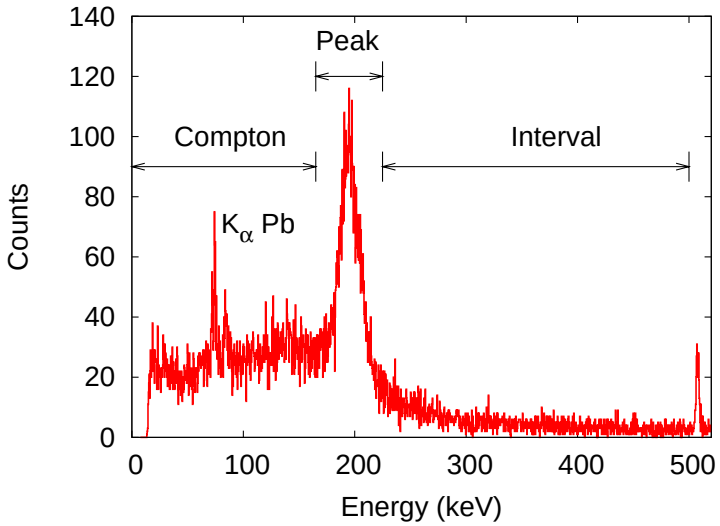

FIG. 18. Backscattering spectrum

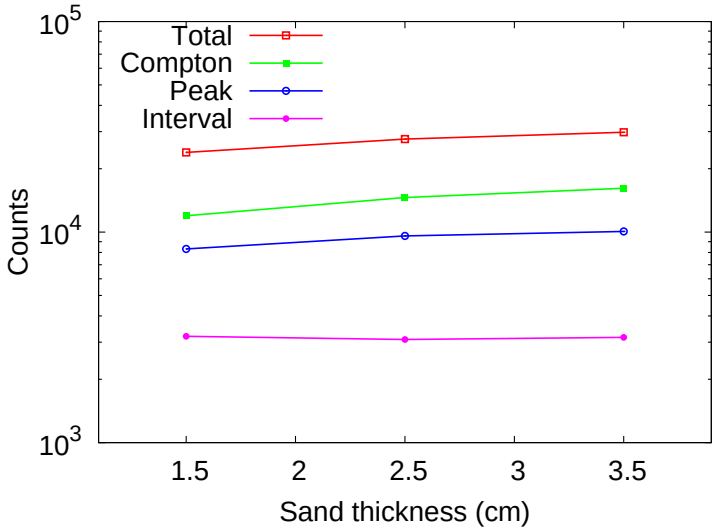

FIG. 19. Number of counts as a function of sand thickness for the regions of the backscattering spectrum

with the larger number of scattering centers. In the case of the interval region there is no observable effect. More detailed study of the behavior of the number of counts as a function of depth needs additionally data for more d values.

In spite of the lack of enough data Figure 20 shows that even for small variations in the sand thickness we are able to observe differences in the backscattering spectra.

Even with the few data that we have collected, the spectra show the possibility of studying the soil composition based on backscattering. However there are several parameters to vary and several studies to be made before being able to state any conclusion.

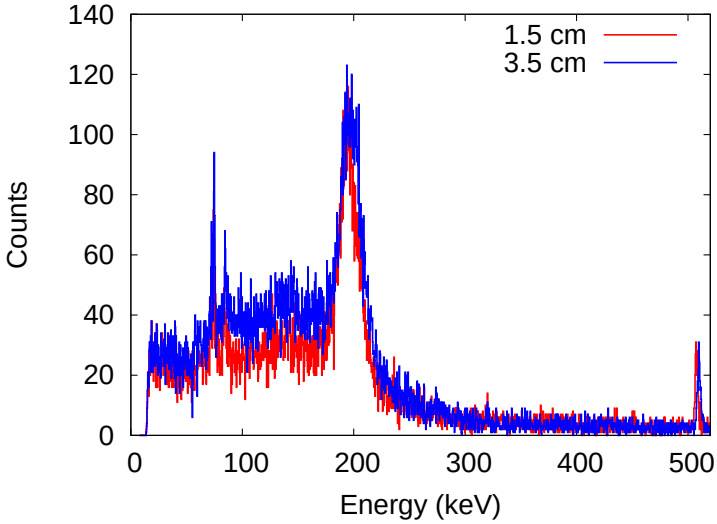

FIG. 20. Comparison of backscattering spectra for two differnt soil thickness

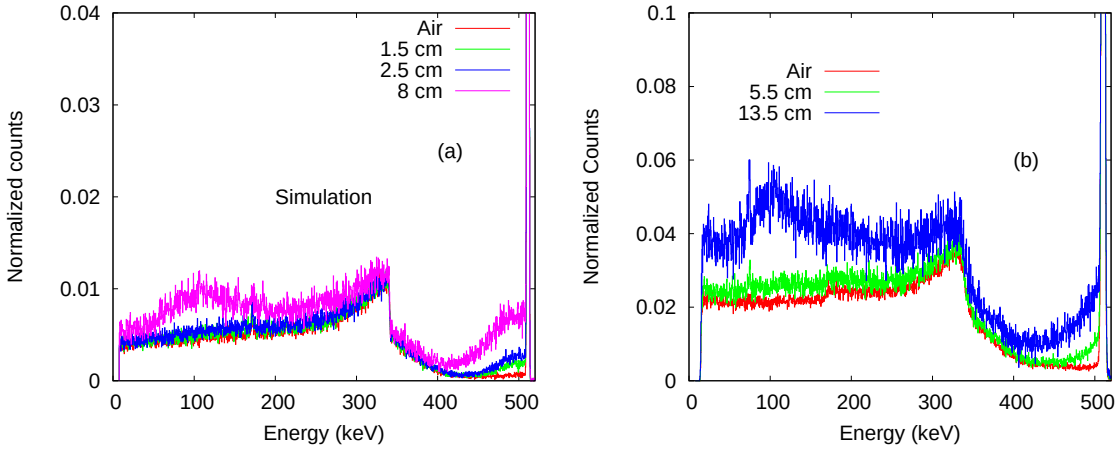

FIG. 21. Comparison of the transmission spectrums obtained experimentally ans by simulation. (a) Simulated spectra for different thickness of soil. (b) Experimental transmission spectra

V. COMPARISON WITH SIMULATION

As an attempt to be able to predict the transmission and the backscattering spectra a comparison with `Geant4` simulations was carried out.

Figure 21 shows a comparison between the simulated transmission spectrum and the experimental result.

This comparison shows that although the overall behavior of the simulated spectra is similar to the experimental ones, there are some differences. For example, although the backscattering peak position is in good agreement in both spectra there is a clear difference in the shape of the Compton region. There are also differences in the shape of the Compton edge and in the tail of the 511 keV photopeak.

Figure 22 shows the backscattering spectrum obtained for a simulation of 2 cm of sand. This spectrum presents many differences with the experimental spectra too. One of the more visible differences is the absence of the characteristic lines of lead in the simulated spectrum. We also notice in this spectrum the absence of the 511 keV peak. Both of these differences evidence that there are missing physical effects in the simulation. In order to be able to make a valid

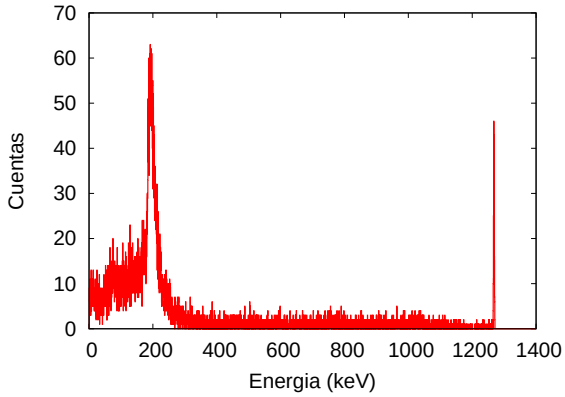

FIG. 22. Simulated backscattering spectrum for 2 cm of sand

comparison we need to improve the simulation.

Figure 22 also shows a strong peak at 1275 keV. The experimental spectra do not present this peak, but this is due to restrictions imposed in the electronic configuration.

VI. CONCLUSIONS

According with an analytical model the effect of beam attenuation is to reduce in two orders of magnitud the number of scattered photons. Nevertheless this calculation neglects the contribution of multiple scattering in the soil. The shape of the experimental spectra for both transmission and backscattering shows a dependence with the thickness of sand layer with which the radiation interacts. From the transmission spectra we obtain an attenuation coefficient for the sand of 0.131(3) cm^{-1}. The difference between this value and the reported for SiO_2 is 1.5%. By normalizing the transmission spectra to the photopeak amplitude we can observe qualitatively the effect due to small–angle scattering in sand. We also saw that the decrease in the number of counts in different parts of the transmission spectrum are due not only to the attenuation of the beam, and we found a change in the behavior of the spectra for sand thickness larger than 12 cm. We found that for thickness larger than 5 cm the backscattering spectra show no difference. In this spectra we observed a peak around 190 keV, which is the result of the combination of various effects, for example multiple scattering of the photons in the sand and the finite size of the detector. The comparison of spectra both of transmission and backscattering shows a overall similar behavior, but also shows the need of an improvement in the simulation.

VII. OUTLOOK

What we have done until this report is only the first step in the understanding of the γ–soil interaction. The next step is to get a better data statistics, and to perform a better analysis of the spectra already obtained.

VIII. ACKNOWLEDGEMENTS

We would like to thank the grupo de física nuclear de la Universidad Nacional (gfnun), the Universidad Nacional de Colombia and the Centro Internacional de Física (CIF).

---

[1] J. Gerl, Nucl. Phys. **A752**, 688c (2005)

[2] http://www.physics.nist.gov/PhysRefData/Xcom/Text/XCOM.html